ACS OMEGA

Open Access

http://pubs.acs.org/journal/acsodf

Article

Point Defects in Silicon-Doped β-Ga_2O_3: Hybrid-DFT Calculations

Published as part of ACS Omega virtual special issue "Jaszowiec 2023".

Asiyeh Shokri,* Yevgen Melikhov, Yevgen Syryanyy, and Iraida N. Demchenko

Cite This: *ACS Omega* 2023, 8, 43732−43738

Read Online

ACCESS | Metrics & More | Article Recommendations | Supporting Information

ABSTRACT: In this work, hybrid density functional theory calculations are used to evaluate the structural and electronic properties and formation energies of Si-doped β-Ga_2O_3. Overall, eight interstitial (Si_i) and two substitutional (Si_{Ga}) positions are considered. In general, our results indicate that the formation energy of such systems is significantly influenced by the charge state of the defect. It is confirmed that it is energetically more favorable for the substitution process to proceed under Ga-poor growth conditions than under Ga-rich growth conditions. Furthermore, it is confirmed that the formation of Si_{GaI} with a tetrahedral coordination geometry is more favorable than the formation of Si_{GaII} with an octahedral one. Out of all considered interstitial positions, due to the negative formation energy of the Si +3 charge state at i_8 and i_9 interstitial positions over the wide range of Fermi energy, this type of defect can be spontaneously stable. Finally, due to a local distortion caused by the presence of the interstitial atom as well as its charge state, these systems obtain a spin-polarized ground state with a noticeable magnetic moment.

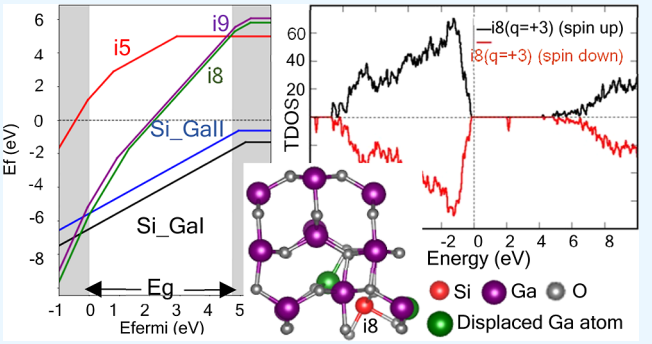

1. INTRODUCTION

In recent years, the monoclinic phase of gallium oxide, known as β-Ga_2O_3, has gained significant attention and importance in various fields due to its exceptional properties and versatile applications. With a band gap value typically falling within the range of 4.5−4.9 eV,[1−4] the thermally stable β-Ga_2O_3 phase holds great promise for revolutionizing diverse areas, ranging from electronics to optoelectronics. This phase has found particular significance in the development of cutting-edge devices, including Schottky barrier diodes,[5,6] metal-oxide-semiconductor field-effect transistors (MOSFETs),[7] metal−semiconductor field-effect transistors,[8] solar-blind photodetectors,[9] resistance random access memory devices,[10] gas sensors,[11] and spintronic devices.[12] Furthermore, the remarkable properties and potential applications of the monoclinic phase of gallium oxide position it as a game-changing material in the field of power electronics, poised to revolutionize the power electronics industry.[7]

Defects in the crystal structure can significantly affect the performance and reliability of devices based on Ga_2O_3.[13] In the monoclinic compound with low symmetry, several point defects need to be considered for vacancy and substitution studies, and in addition, interstitial sites, which can be occupied by neutral or charged atoms, must also be considered. According to the literature, some primary defects are considered to be electrically active. For example, gallium vacancies (V_{Ga}), as well as their complexes with hydrogen, are deep acceptors, but gallium interstitial (with just one of the lowest formation energies the authors have found), Ga_i,[14] is a shallow donor. On the other hand, the oxygen vacancy and interstitial are expected to be deep donors and hence electrically neutral for Fermi-level positions close to the conduction band minimum (CBM).[14−16]

Dopants also play a crucial role in modifying the electrical and optical properties of the material, enabling the creation of specific device functionalities. By carefully selecting and controlling dopants, it is possible to tailor the conductivity type (n-type or p-type) and achieve the desired carrier concentration in gallium oxide. The ability to precisely dope β-Ga_2O_3 with impurities such as Sn, Si, Ge, and Mg enables the realization of high-quality n-type epitaxial films, offering a wide range of electron densities from 1×10^{16} to 1×10^{19} cm^{-3}. Theoretical calculations indicate that Si, Ge, and Sn serve as the most common shallow donor impurities, with Si predicted to be the shallowest donor among them.[17] Recent *ab initio* study of complexes of substitutional defects shows that doping Ga_2O_3 with Si could lead to an acceptor with Si_O coupled with

Received: July 30, 2023
Revised: October 24, 2023
Accepted: October 26, 2023
Published: November 9, 2023

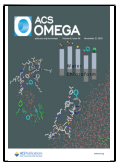

H_{Ga} or to a donor with Si_{Ga}.[18] Despite extensive research on Si doping in β-Ga_2O_3 and the preference for Si substitution at the Ga_I site rather than at the interstitial positions,[15,16] a comprehensive study of the various possible interstitial positions, their formation energy, and the replacement of intrinsic atoms as a result of interstitial doping is still lacking.

One of the reasons for the absence of such studies has been the understanding that in the case of Si interstitials, in a thermodynamically stable condition, only a small concentration of Si_i atoms would be present due to the negative formation energy of Si_{Ga}.[18] However, the situation could change dramatically when a suitable out-of-equilibrium growth technique, such as ion implantation doping, is used. In this case, due to the ballistic nature of this process, the buildup of a lattice disorder occurs and it is accompanied by the formation of various types of defects in relatively large concentrations. Recent experimental studies of β-Ga_2O_3:Si system prepared by ion implantation with Si ions show that Si interstitials occur in large concentration but not as isolated atoms but as complexes of Si_i with gallium and/or oxygen vacancies.[19] Thus, to better understand the changes in the properties of β-Ga_2O_3 and gallium oxide-based materials, the most favorable interstitial sites should be identified through further analysis and simulations.

In the study by Blanco et al.,[20] a comprehensive theoretical investigation of point defects in β-Ga_2O_3 was carried out, focusing on the ionic conductivity of the material. The energetics and diffusion properties of both the host lattice and dopant ions in β-Ga_2O_3 were examined within the framework of the shell model. Overall, eight different optimum configurations were identified for the Ga interstitials. Then, specifically for the Si dopant, the researchers adopted an ionic description considering Si^{4+}. Such an approach assumes that the electronic distributions of positively charged ions do not undergo significant changes upon incorporation of ions into the lattice of β-Ga_2O_3. This simplification allowed for a more straightforward treatment of the dopant and facilitated the analysis of its behavior within the crystal structure.

In this article, we explore the doping properties of Si in the monoclinic phase of gallium oxide. Specifically, we investigate the formation energies of Si in eight interstitial sites and two distinct substitutional sites (Ga_I and Ga_{II}). Our objective in this work is to analyze the relaxed positions and behavior of the Si dopants, calculate transition energies, and examine their impact on the electronic structure and optical properties of the pristine material.

2. COMPUTATIONAL METHODS

In this study, the first-principles density functional theory (DFT) calculations have been performed using the Vienna *ab initio* simulation package (VASP, v. 6.3.2) with projector augmented wave potentials.[21−24] To accurately capture the structural and electronic properties of β-Ga_2O_3, the HSE06 hybrid functional[25] was employed. This functional incorporates a fraction of exact exchange (0.32)[26] and a fixed screening parameter of 0.2 $Å^{-1}$. All calculations were spin polarized. The formation energy of an impurity with charge state q can be calculated using[27]

$$E_q^f = E_{tot}(X_q) - E_{tot}(\text{bulk}) - \sum_i n_i \cdot \mu_i + q \cdot (E_{VBM} + E_F) + E_{corr} \quad (1)$$

Here, $E_{tot}(X_q)$ represents the total energy of the supercell containing the defect in charge state q, and E_{tot}(bulk) denotes the total energy of the defect-free crystal. n_i represents the change in the number of atoms due to the formation of a defect: it is negative if the atom of the i-th species is removed and positive in case an atom of the i-th species is added. The term $q\cdot(E_{VBM} + E_F)$ accounts for the energy change upon the removal or addition of electrons during the formation of charged defects, with E_F representing the Fermi energy of β-Ga_2O_3 and E_{VBM} being the valence band maximum (VBM) value. To account for the elimination of false electrostatic interactions between charged defect supercells, the Freysoldt−Neugebauer−Van de Walle correction term, E_{corr}, was included.[28] The experimental value of 10 is taken for the dielectric constant.[29] The chemical potentials μ_i of the elements calculated in this work are −5.69 eV for Si (from Si bulk), −3.38 eV for Ga (bulk Ga metal), and −7.187 eV for O (O_2 molecules), enabling the determination of the Ga-rich (O-poor) and Ga-poor (O-rich) limits based on the enthalpy of formation of β-Ga_2O_3.

To construct the formation energy curve for a chosen defect, it is necessary to perform calculations according to eq 1 for a set of charge states q (typical values for q are 0, ±1, ±2, and ±3), considering the Fermi energy E_F as an independent variable in eq 1. Then, by varying E_F, it is possible to identify the charge state q^* that has the lowest formation energy $E_{q^*}^f$ among all of the studied charges at that particular value of E_F. By plotting values of $E_{q^*}^f$ as a function of E_F, the formation energy curve for a chosen defect is constructed.[30,31] The resulting formation energy curve will be a piecewise linear function, with each segment corresponding to a particular slope associated with the charge that is most stable (favorable) at the given interval of the Fermi energy E_F of that segment.

An additional parameter can be extracted from eq 1 and/or from the formation energy curve directly, i.e., a thermodynamic charge transition level (the position of the Fermi energy where q_1 and q_2 charge states have equivalent formation energies), which can be calculated using[32]

$$\varepsilon(q_1/q_2) = \frac{E_{q_1}^f|_{E_F=0} - E_{q_2}^f|_{E_F=0}}{q_2 - q_1} \quad (2)$$

Here, $E_q^f|_{E_F=0}$ represents the formation energy of the defect in charge state q considered at $E_F = 0$.

3. RESULTS AND DISCUSSION

The monoclinic crystal structure of β-Ga_2O_3 belongs to the $C2/m$ space group and consists of 20 atoms in the conventional unit cell. To determine the optimized lattice constants for the pristine β-Ga_2O_3 (Figure 1), energy minimization calculations were first performed for different volumes of the 20-atom unit cell. Then, optimization of the lattice constants was carried out under the constant optimized volume condition, yielding values of a = 12.22 Å, b = 3.303 Å, and c = 5.79 Å for pristine β-Ga_2O_3. These values, as well as other obtained parameters, are in good agreement with those reported in the literature obtained from *ab initio* calculations and from experiments (see Table 1).

For the calculation of formation energies of interstitial and substitutional defects, a 160-atoms 1 × 4 × 2 supercell was created that has a size of a = 12.22 Å, b = 12.22 Å, and c = 11.58 Å. The choice of such a supercell guaranteed that the

https://doi.org/10.1021/acsomega.3c05557
ACS Omega 2023, 8, 43732−43738

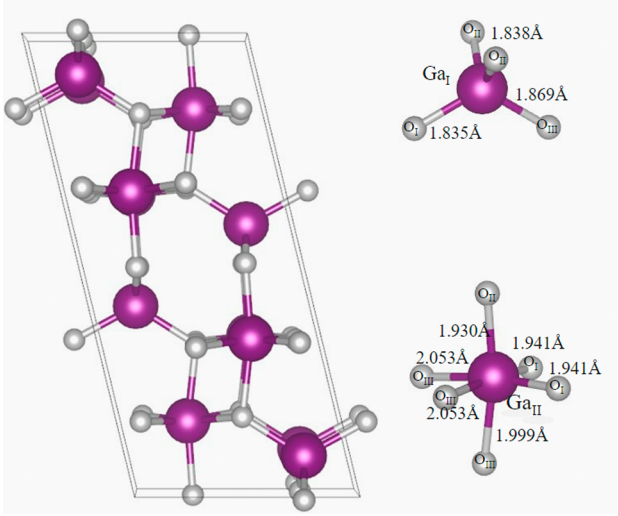

Figure 1. Unit cell of the monoclinic phase of Ga_2O_3. Coordination environment of tetrahedral Ga_I and octahedral Ga_{II} positions (purple spheres are Ga atoms; gray spheres are O atoms).

Table 1. Lattice Constants, Band Gap Energy, and Formation Enthalpy of β-Ga_2O_3 (ΔE) Resulting from GGA and HSE Calculations from This Work and Compared with Experimental and Theoretical Results Found in the Literature[a]

	GGA	GGA (a)	HSE06	HSE06 (b)	exp
a (Å)	12.452	12.446	12.221	12.253	12.214 (c)
b (Å)	3.082	3.083	3.028	3.034	3.037 (c)
c (Å)	5.876	5.876	5.792	5.789	5.798 (c)
β (deg)	103.68	103.70	103.79	103.80	103.83 (c)
E_g (eV)	2.05	2.0	4.73	4.7	4.9 (d)
ΔE (eV)	−9.43	−9.3	−12.23	−10.3	−11.3 (e)

[a]note: (a) ref 33 (b) ref 34 (c) ref 35 (d) ref 36 (e) ref 35.

average interdefect distance is large enough to ensure that the error in the formation energy is small and, in addition, that this distance is approximately the same in all directions to avoid any unnecessary bias during relaxation.[14,33] An energy cutoff of 510 eV was chosen along with a 2 × 8 × 4 Γ-centered Monkhorst−Pack[37] k-point grid for the unit cell. For computations on the supercell, single Γ-point calculations were performed for all interstitial cases, and a 2 × 2 × 2 Γ-centered Monkhorst−Pack k-point grid was used for calculations on a few selected cases. The convergence criteria were set so that the forces on each ion were less than 0.03 eV $Å^{-1}$ and the total energy changes were reduced to less than 1×10^{-4} eV per atom.

As was mentioned above, the crystal structure of β-Ga_2O_3 comprises two inequivalent Ga sites (Ga_I and Ga_{II}) and three inequivalent oxygen sites (O_I, O_{II}, and O_{III}). Figure 1 illustrates the coordination environment of these atoms, where Ga_I and Ga_{II} are coordinated by four (tetrahedral) and six (octahedral) oxygen atoms, respectively. Note that there are three inequivalent positions for oxygen: O_I is coordinated by two Ga_{II} and one Ga_I, and O_{II} is coordinated by two Ga_I and one Ga_{II}, while O_{III} is coordinated by four atoms. The bond lengths between different atoms are also depicted in Figure 1.

Altogether, there were eight different initial positions, denoted as i_1, i_2, i_3, i_4, i_5, i_6, i_8, and i_9, considered for the initial position of interstitial Si atoms (see Supporting Information for a graphical visualization of these eight initial positions used in interstitial calculations). Here, the notation from ref 20 is used to identify the interstitial positions. Note that the initial position i_7, as well as positions i_{10} and i_{11} were excluded from consideration as they were shown to be energetically unstable.[20] The systems with doped atoms in these eight positions were then relaxed to determine the most stable configuration for interstitial Si atoms in their neutral states in the crystal lattice. Then, using a single Γ-point for a k-point grid, the formation energies of neutral Si interstitials were computed to identify the most promising cases of interstitial defects for further analysis. Table 2 shows that the formation

Table 2. Formation Energy E^f of the Neutral (q = 0) Si Interstitial at Different Locations, Sorted in Ascending Order[a]

	E^f (eV)
Si_{i8}	4.74
Si_{i9}	5.00
Si_{i5}	5.30
Si_{i1}	8.28
Si_{i4}	9.01
Si_{i2}	9.40
Si_{i3}	10.37
Si_{i6}	15.10

[a]Note that the calculations were performed on a large supercell but with a single Γ-point as k-point grid.

energies for the Si interstitial at three positions, i_8, i_9, and i_5, are close to each other and have values that are much lower than the values for other cases. These three positions, i_8, i_9, and i_5, were selected for further analysis with more accurate computations (denser k-point grid) and with charged defects. The charge of the supercell was set to take the values 0, +1, +2, +3, and +4 for each defect in these cases.

Let us start the discussion with the formation energy results. As shown in Figure 2, Si substitution at the Ga_I site is energetically more favorable than that at the Ga_{II}. For both defects, the charge state +1 is the stable one. The obtained results agree well with the literature data.[16] Slight deviations in numerical values are attributed to the different functionals used (HSE06 hybrid functional[25,26] in this work vs PBE0 hybrid functional[38,39] in[16]) as well as to the different supercells used (160 atoms in this work vs 120 atoms in ref 16). For the considered host matrix, the substitutional Si_{Ga} defects at the Ga_I and Ga_{II} sites are energetically more favorable than the interstitial Si_i defects over the whole band gap range and for both Ga-rich and Ga-poor conditions. Only in the case of Ga-rich conditions and for Fermi energies very close to the VBM, the formation energy of the interstitial Si at position i_8 is slightly lower than the value for the substitutional Si_{Ga} at the Ga_{II} site.

For Si placed at interstitial positions, our calculations reveal that for all defects studied, the dependence of the formation energy on the Fermi energy is not monotonic, i.e., their charge state changes depending on the current level of the Fermi energy. For example, the charge state +3 is the favorable state for Si placed at the interstitial positions i8 from the VBM to 1.32 eV, and after that the charge state +2 is the favorable state. A similar dependence, with a similar value of the transition level, is observed for Si placed at interstitial positions i_9. In case Si placed at the interstitial position i_5, the neutral state could

https://doi.org/10.1021/acsomega.3c05557
ACS Omega 2023, 8, 43732−43738

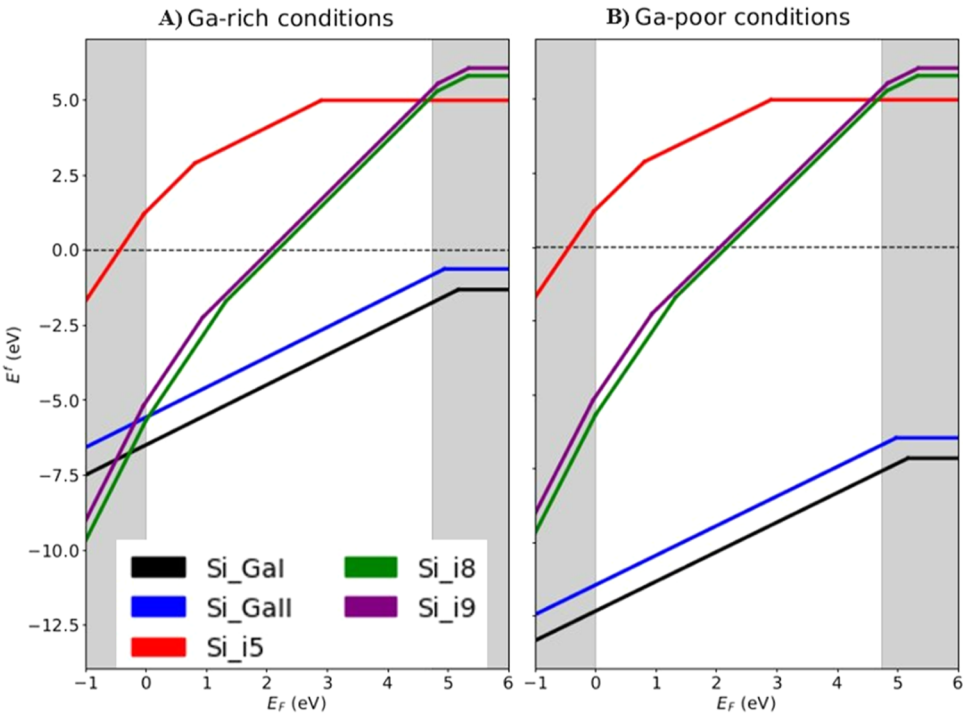

Figure 2. Formation energies for Si impurity in β-Ga_2O_3 plotted against the Fermi energy for (A) Ga-rich and (B) Ga-poor conditions. The boundaries for the nonshaded region correspond to the VBM (E_F = 0 eV) and the CBM ($E_F = E_g$ = 4.73 eV). Note that the calculations were performed on a large supercell with a dense k-point grid.

also be favorable for the higher E_F values. Overall, Si placed at interstitial positions i_8 and i_9 is more energetically favorable than Si placed at interstitial position i_5 over the whole band gap range. Only for Fermi energies very close to the CBM, the formation energy of the interstitial Si at the position i_5 is lower than for the interstitial Si at positions i_8 and i_9; hence, the Si_{i5} case is more favorable. Table 3 indicates the thermodynamic energy transition between different charge states for each considered defect. It is also worth noting that all considered structures correspond to positive charge states in the energy band gap region (and neutral for Si_{i5} at higher E_F values), indicating that these interstitial defects could only act as donors.

Table 3. Transition Level $\varepsilon(q_1/q_2)$ for Si-Doped β-Ga_2O_3 in the Range of E_F is Presented in Figure 2[a]

	+1/0	+2/+1	+3/+2	+4/+3
Si_{i8}	5.33	4.82	1.32	-0.01
Si_{i9}	5.34	4.83	0.93	-0.25
Si_{i5}	2.90	0.81	-0.10	-
Si_{GaI}	5.17	-	-	-
Si_{GaII}	4.97	-	-	-

[a]The shaded cells indicate values outside of the band gap range ($0 \le E_F \le E_g$ = 4.73 eV). Missing values denote transitions absent within the range of E_F presented in Figure 2 ($-1 \le E_F \le 6$ eV).

To the best of our knowledge, there were only a few theoretical studies on Si interstitial in β-Ga_2O_3,[16,18,20] with only one study that looked into different charge states of Si interstitial.[16] Qualitatively, the formation energy curves for Si placed at the interstitial positions i_8 and i_9 are similar to the curve for Si interstitial presented in ref 16 (see Figure 1 therein): the formation energy changes from the value of −9 eV at the VBM to the value + 5 eV at the CBM, crossing E^F = 0 eV somewhere in the middle of the band gap, and having stable charges +1, +2, and +3. Quantitatively, however, there are changes due to differences in the values of the transition levels +3/+2 and +2/+1, which are attributed to different functionals and supercells used as discussed earlier.

Finally, note also that the formation energy values of neutral defects calculated using a denser k-point grid differ significantly from those calculated using only a single Γ-point. It can also be seen from Table 2 and Figure 2 that even the order of the values is different for Si_{i5}, Si_{i8}, and Si_{i9}. This confirms the fact that DFT calculations should be carefully checked not only with respect to the supercell size but also with respect to the k-point mesh. One should also keep in mind that, for a chosen Si interstitial case, the relaxation is performed for the neutral state only in this work. The resulting relaxed structures were then used as fixed structures for computations with charged defects. This is a standard approach where it is assumed that the doping procedure or any subsequent treatment steps do not allow for the host matrix to be further relaxed. However, in the future, depending on the conditions, a relaxation procedure may also need to be performed for charged defects.

For all of the studied cases, it was found that the interstitial defects led to some structural reorganization through displacing neighboring O and Ga atoms out of their initial sites. Figure 3 demonstrates the final position of the interstitial atoms and their neighbors for the cases i_5, i_8, and i_9. The case i_5 showed the least change in the initial structure after relaxation. In this case, the Si interstitial did not move from its initial position, and the neighboring atoms of O and Ga were displaced by a maximum of 0.30 Å. In the case i_8, the Si interstitial moved from its initial position by 0.35 Å; however,

https://doi.org/10.1021/acsomega.3c05557
ACS Omega 2023, 8, 43732−43738

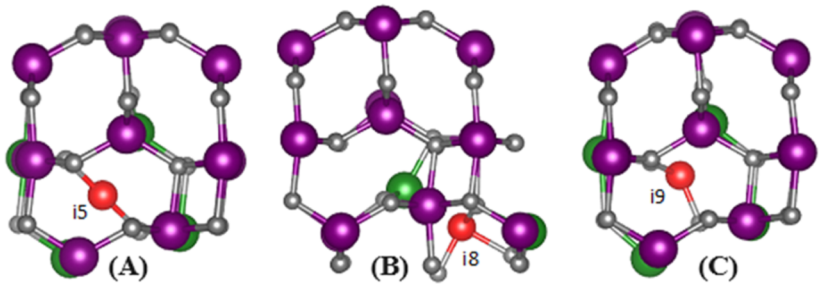

Figure 3. Positions of atoms after relaxation for doped β-Ga_2O_3 with Si interstitial at positions (A) i_5, (B) i_8, and (C) i_9. Note: The red spheres denote Si atoms, gray spheres oxygen (O) atoms, purple spheres gallium (Ga) atoms, and green spheres indicate the Ga atoms shifted most substantially during structural relaxation.

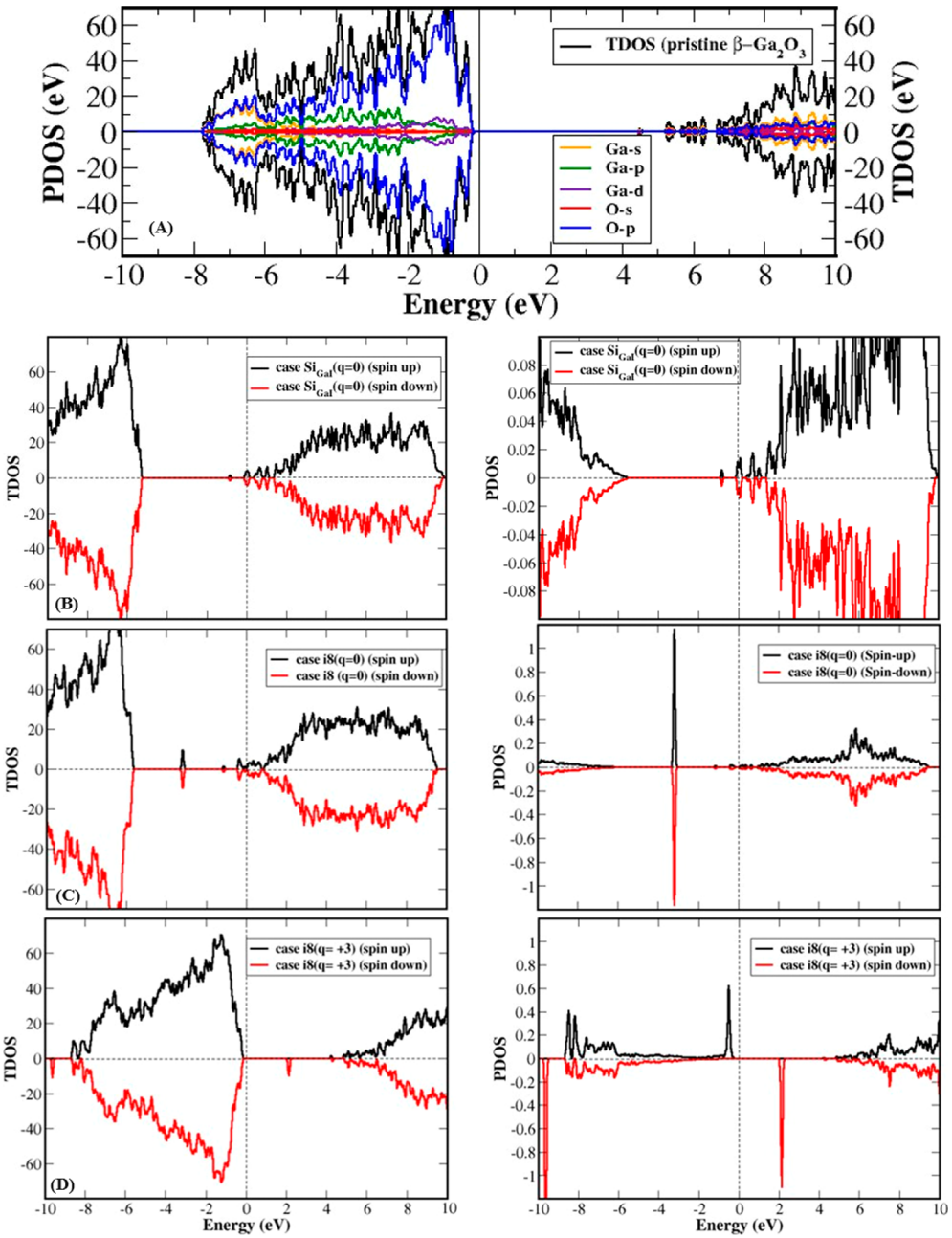

Figure 4. TDOS and PDOS for the cases of (A) pristine β-Ga_2O_3, (B) substitutional Si at the Ga_I site, (C) neutral Si interstitial at the i_8 position, and (D) +3 charge state Si interstitial at the i_8 position (the Fermi energy is set to 0 eV).

https://doi.org/10.1021/acsomega.3c05557
ACS Omega 2023, 8, 43732−43738

one of the atoms of Ga was displaced by 0.92 Å with the rest of the neighboring atoms of O and Ga by a maximum of 0.35 Å. Finally, in the case i_9, the Si interstitial was displaced by 0.60 Å from its initial position, which is the largest displacement of Si interstitial among the studied cases. The neighboring atoms of O and Ga were also displaced by a maximum of 0.30 Å, as in the case of i_5. Some of the coordinates and distances for these cases are given in Table S3 in the Supporting Information.

The calculated density of states (DOS) for the pristine sample, that is, the intrinsic β-Ga_2O_3, is shown in Figure 4A, with a band gap of 4.73 eV. The VBM clearly corresponds mainly to the O 2p states. The substitution of Si at the Ga_I site (Si_{GaI}), which is the most favorable of the two substitution cases, causes the material to exhibit metallic behavior, as shown in Figure 4B. Figure 4C,D presents the total DOSs (TDOS) and partial DOSs (PDOS) for Si interstitial at position i_8 with charge states +2 and +3. This choice is based on the fact that case i_8 has the lowest formation energy over almost the entire Fermi energy range from the CBM to the VBM, and charge states +2 and +3 are the most stable (favorable) states near the CBM and the VBM, respectively. The TDOS and PDOS for cases i_9 and i_5 are provided in Supporting Information. Near the VBM, for interstitials at positions i_8 (+3 charge), i_9 (+3 charge), and i_5 (+2 charge), the system remains a semiconductor with E_g of 2.076, 1.780, and 1.191 eV, respectively. Near the CBM, for interstitials at positions i_8 (+2 charge), i_9 (+2 charge), and i_5 (neutral), the system is also a semiconductor with E_g of 2.24, 2.44, and 1.61 eV, respectively. Finally, it is worth mentioning that the charge states induce magnetic moments of 1.00 μ_B for the cases i_8 (+3 charge) and i_9 (+3 charge), 2.00 μ_B for the case i_5 (+2 charge) but 0.00 μ_B for the case i_8 (+2 charge) and i_9 (+2 charge). The magnetic moment is absent for the case i_5 (neutral). The appearance of magnetic moment can be attributed to the displacement of Ga neighbors, as previously demonstrated in a study by Yang et al.,[40] which showed that vacancies of Ga_I and Ga_{II} can induce magnetism in the monoclinic phase of Ga_2O_3.

4. CONCLUSIONS

In this work, we utilized a DFT approach with a hybrid functional to study various point defects, such as interstitial and substitutional Si, in the low-symmetric monoclinic phase of Ga_2O_3. Our results indicate that in the case of substituting, the Si atom mostly prefers the Ga_I site that agrees well with the literature. In the case of eight different interstitial Si point defects studied here, first, the cases i_8, i_9, and i_5 were selected based on their lower formation energy of defects at neutral charge computed at Γ-point only. Then, these cases were analyzed at different charges, selecting the most favorable among them. We found that among the studied interstitial defects, the case with Si positioned at i_8 is the most favorable over the entire Fermi level range but could be at different charge states: +3 near the VBM and +2 near the CBM. In addition, our results show that these defects at the charge state induce a noticeable spin polarization, keeping semiconducting properties.

■ ASSOCIATED CONTENT

Data Availability Statement

The data that support the findings of this study are publicly available at 10.18150/1MQF0J.

Supporting Information

The Supporting Information is available free of charge at https://pubs.acs.org/doi/10.1021/acsomega.3c05557.

Crystal structure of β-Ga_2O_3 with marked different initial positions for interstitial atoms; TDOS and PDOS for doped β-Ga_2O_3 with neutral and charged interstitial defects for different cases; and initial and final after-relaxation procedure positions of the atoms with the largest displacement for different cases (PDF)

■ AUTHOR INFORMATION

Corresponding Author

Asiyeh Shokri − *Institute of Plasma Physics and Laser Microfusion, 01-497 Warsaw, Poland;* orcid.org/0000-0002-8574-4353; Email: asiye.shokri@gmail.com, asiyeh.shokri@ifpilm.pl

Authors

Yevgen Melikhov − *Institute of Fundamental Technological Research Polish Academy of Sciences, 02-106 Warsaw, Poland*

Yevgen Syryanyy − *Institute of Plasma Physics and Laser Microfusion, 01-497 Warsaw, Poland; Institute of Microelectronics and Optoelectronics, Warsaw University of Technology, 00-662 Warsaw, Poland*

Iraida N. Demchenko − *Institute of Plasma Physics and Laser Microfusion, 01-497 Warsaw, Poland*

Complete contact information is available at: https://pubs.acs.org/10.1021/acsomega.3c05557

Notes

The authors declare no competing financial interest.

■ ACKNOWLEDGMENTS

The work was partially supported by the Interdisciplinary Centre for Mathematical and Computational Modelling (ICM) at University of Warsaw, Poland, grant ID 3557. We gratefully acknowledge Poland's high-performance Infrastructure PLGrid (HPC Centers: ACK Cyfronet AGH, PCSS, CI TASK, WCSS) for providing computer facilities and support within computational grant no PLG/2023/016578. These studies were financially supported by the project UMO-2020/39/B/ST5/03580 founded by the National Science Centre (NCN) in Poland.

■ REFERENCES

(1) Ueda, N.; Hosono, H.; Waseda, R.; Kawazoe, H. Anisotropy of Electrical and Optical Properties in β-Ga2O3 Single Crystals. *Appl. Phys. Lett.* **1997**, *71* (7), 933−935.

(2) Janowitz, C.; Scherer, V.; Mohamed, M.; Krapf, A.; Dwelk, H.; Manzke, R.; Galazka, Z.; Uecker, R.; Irmscher, K.; Fornari, R.; Michling, M.; Schmeißer, D.; Weber, J. R.; Varley, J. B.; Walle, C. G. V. d. Experimental Electronic Structure of In2O3 and Ga2O3. *New J. Phys.* **2011**, *13*, 085014.

(3) Tippins, H. H. Optical Absorption and Photoconductivity in the Band Edge of β-Ga2O3. *Phys. Rev.* **1965**, *140* (1A), A316−A319.

(4) Ingebrigtsen, M. E.; Varley, J. B.; Kuznetsov, A. Y.; Svensson, B. G.; Alfieri, G.; Mihaila, A.; Badstübner, U.; Vines, L. Iron and Intrinsic Deep Level States in Ga2O3. *Appl. Phys. Lett.* **2018**, *112* (4), 42104.

(5) Mohamed, M.; Irmscher, K.; Janowitz, C.; Galazka, Z.; Manzke, R.; Fornari, R. Schottky Barrier Height of Au on the Transparent Semiconducting Oxide β-Ga2O3. *Appl. Phys. Lett.* **2012**, *101*(13), 132106.

(6) Oda, M.; Tokuda, R.; Kambara, H.; Tanikawa, T.; Sasaki, T.; Hitora, T. Schottky barrier diodes of corundum-structured gallium oxide showing on-resistance of 0.1 mΩ·cm^2 grown by MIST EPITAXY. *Appl. Phys. Express* **2016**, *9* (2), 021101.
(7) Higashiwaki, M.; Sasaki, K.; Kamimura, T.; Hoi Wong, M.; Krishnamurthy, D.; Kuramata, A.; Masui, T.; Yamakoshi, S. Depletion-Mode Ga2O3Metal-Oxide-Semiconductor Field-Effect Transistors on β-Ga2O3 (010) Substrates and Temperature Dependence of Their Device Characteristics. *Appl. Phys. Lett.* **2013**, *103*, 123511.
(8) Higashiwaki, M.; Sasaki, K.; Kuramata, A.; Masui, T.; Yamakoshi, S. Gallium Oxide (Ga2O3) Metal-Semiconductor Field-Effect Transistors on Single-Crystal β-Ga2O3 (010) Substrates. *Appl. Phys. Lett.* **2012**, *100* (1), 13504.
(9) Suzuki, R.; Nakagomi, S.; Kokubun, Y.; Arai, N.; Ohira, S. Enhancement of Responsivity in Solar-Blind β-Ga2O3 Photodiodes with a Au Schottky Contact Fabricated on Single Crystal Substrates by Annealing. *Appl. Phys. Lett.* **2009**, *94* (22), 222102.
(10) Dong, L.; Jia, R.; Li, C.; Xin, B.; Zhang, Y. Ab Initio Study of N-Doped β-Ga2O3 with Intrinsic Defects: The Structural, Electronic and Optical Properties. *J. Alloys Compd.* **2017**, *712* (712), 379−385.
(11) Ogita, M.; Higo, K.; Nakanishi, Y.; Hatanaka, Y. Ga2O3 Thin Film for Oxygen Sensor at High Temperature. *Appl. Surf. Sci.* **2001**, *175*−*176*, 721−725.
(12) Guo, D.; Wu, Z.; An, Y.; Li, X.; Guo, X.; Chu, X.; Sun, C.; Lei, M.; Li, L.; Cao, L.; Li, P.; Tang, W. Room Temperature Ferromagnetism in (Ga1-xMnx)2O3 Epitaxial Thin Films. *J. Mater. Chem. C* **2015**, *3* (8), 1830−1834.
(13) Welch, E.; Borges, P.; Scolfaro, L. Hybrid Density Functional Theory Study of Substitutional Gd in β-Ga2O3. *Phys. B* **2023**, *651*, 414558.
(14) Deák, P.; Duy Ho, Q.; Seemann, F.; Aradi, B.; Lorke, M.; Frauenheim, T. Choosing the Correct Hybrid for Defect Calculations: A Case Study on Intrinsic Carrier Trapping in β-Ga2O3. *Phys. Rev. B* **2017**, *95* (7), 075208.
(15) Varley, J. B.; Weber, J. R.; Janotti, A.; Van De Walle, C. G. Oxygen Vacancies and Donor Impurities in β-Ga2O3. *Appl. Phys. Lett.* **2010**, *97* (14), 142106.
(16) Bouzid, A.; Pasquarello, A. Defect Formation Energies of Interstitial C, Si, and Ge Impurities in β-Ga2O3. *Phys. Status Solidi RRL* **2019**, *13* (8), 1800633.
(17) Lany, S. Defect Phase Diagram for Doping of Ga2O3. *APL Mater.* **2018**, *6* (4), 046103.
(18) Zeman, C. J.; Kielar, S. M.; Jones, L. O.; Mosquera, M. A.; Schatz, G. C. Investigation of P-Type Doping in β- and κ-Ga2O3. *J. Alloys Compd.* **2021**, *877*, 160227.
(19) Demchenko, I. N.; Shokri, A.; Melikhov, Y.; Syryanyy, Y. Unpublished Raw X-Ray Absorption Spectroscopy Data. **2023**.
(20) Blanco, M. A.; Sahariah, M. B.; Jiang, H.; Costales, A.; Pandey, R. Energetics and Migration of Point Defects in Ga2O3. *Phys. Rev. B: Condens. Matter Mater. Phys.* **2005**, *72* (18), 184103.
(21) Kresse, G.; Hafner, J. Ab Initio Molecular-Dynamics Simulation of the Liquid-Metal-Amorphous-Semiconductor Transition in Germanium. *Phys. Rev. B: Condens. Matter Mater. Phys.* **1994**, *49* (20), 14251−14269.
(22) Kresse, G.; Furthmüller, J. Efficiency of Ab-Initio Total Energy Calculations for Metals and Semiconductors Using a Plane-Wave Basis Set. *Comput. Mater. Sci.* **1996**, *6* (1), 15−50.
(23) Kresse, G.; Furthmüller, J. Efficient Iterative Schemes for Ab Initio Total-Energy Calculations Using a Plane-Wave Basis Set. *Phys. Rev. B: Condens. Matter Mater. Phys.* **1996**, *54* (16), 11169−11186.
(24) Kresse, G.; Joubert, D. From Ultrasoft Pseudopotentials to the Projector Augmented-Wave Method. *Phys. Rev. B: Condens. Matter Mater. Phys.* **1999**, *59* (3), 1758−1775.
(25) Heyd, J.; Scuseria, G. E.; Ernzerhof, M. Hybrid Functionals Based on a Screened Coulomb Potential. *J. Chem. Phys.* **2003**, *118* (18), 8207−8215.
(26) Lyons, J. L. Electronic Properties of Ga2O3 Polymorphs. *ECS J. Solid State Sci. Technol.* **2019**, *8* (7), Q3226−Q3228.
(27) Freysoldt, C.; Grabowski, B.; Hickel, T.; Neugebauer, J.; Kresse, G.; Janotti, A.; Van De Walle, C. G. First-Principles Calculations for Point Defects in Solids. *Rev. Mod. Phys.* **2014**, *86* (1), 253−305.
(28) Freysoldt, C.; Neugebauer, J.; Van de Walle, C. G. Electrostatic Interactions between Charged Defects in Supercells. *Phys. Status Solidi B* **2011**, *248* (5), 1067−1076.
(29) Passlack, M.; Hunt, N. E. J.; Schubert, E. F.; Zydzik, G. J.; Hong, M.; Mannaerts, J. P.; Opila, R. L.; Fischer, R. J. Dielectric Properties of Electron-beam Deposited Ga2O3 Films. *Appl. Phys. Lett.* **1994**, *64* (20), 2715−2717.
(30) Kyrtsos, A.; Matsubara, M.; Bellotti, E. Migration Mechanisms and Diffusion Barriers of Vacancies in Ga2O3. *Phys. Rev. B* **2017**, *95* (24), 245202.
(31) Broberg, D.; Bystrom, K.; Srivastava, S.; Dahliah, D.; Williamson, B. A. D.; Weston, L.; Scanlon, D. O.; Rignanese, G. M.; Dwaraknath, S.; Varley, J.; Persson, K. A.; Asta, M.; Hautier, G. High-Throughput Calculations of Charged Point Defect Properties with Semi-Local Density Functional Theory—Performance Benchmarks for Materials Screening Applications. *npj Comput. Mater.* **2023**, *9* (1), 72−12.
(32) Kyrtsos, A.; Matsubara, M.; Bellotti, E. On the Feasibility of P-Type Ga2O3. *Appl. Phys. Lett.* **2018**, *112* (3), 32108.
(33) Zacherle, T.; Schmidt, P. C.; Martin, M. Ab Initio Calculations on the Defect Structure of β-Ga2O3. *Phys. Rev. B: Condens. Matter Mater. Phys.* **2013**, *87* (23), 235206.
(34) Varley, J. B.; Weber, J. R.; Janotti, A.; Van De Walle, C. G. Erratum: "Oxygen vacancies and donor impurities in β-Ga2O3" [Appl. Phys. Lett. 97, 142106 (2010)]. *Appl. Phys. Lett.* **2016**, *108* (3), 48.
(35) Åhman, J.; Svensson, G.; Albertsson, J. A Reinvestigation of β-Gallium Oxide. *Acta Crystallogr. C* **1996**, *52* (6), 1336−1338.
(36) Orita, M.; Ohta, H.; Hirano, M.; Hosono, H. Deep-Ultraviolet Transparent Conductive β-Ga2O3 Thin Films. *Appl. Phys. Lett.* **2000**, *77* (25), 4166−4168.
(37) Monkhorst, H. J.; Pack, J. D. Special Points for Brillouin-Zone Integrations. *Phys. Rev. B: Condens. Matter Mater. Phys.* **1976**, *13* (12), 5188−5192.
(38) Adamo, C.; Barone, V. Toward Reliable Density Functional Methods without Adjustable Parameters: The PBE0Model. *J. Chem. Phys.* **1999**, *110* (13), 6158−6170.
(39) Perdew, J. P.; Ernzerhof, M.; Burke, K. Rationale for Mixing Exact Exchange with Density Functional Approximations. *J. Chem. Phys.* **1996**, *105* (22), 9982−9985.
(40) Yang, Y.; Zhang, J.; Hu, S.; Wu, Y.; Zhang, J.; Ren, W.; Cao, S. First-Principles Study of Ga-Vacancy Induced Magnetism in β-Ga2O3. *Phys. Chem. Chem. Phys.* **2017**, *19* (42), 28928−28935.

https://doi.org/10.1021/acsomega.3c05557
ACS Omega 2023, 8, 43732−43738